Modeling of CO_2 plasma : effect of uncertainties in the plasma chemistry

Modeling of CO_2 plasma: Effect of uncertainties in the plasma chemistry

Modeling of CO_2 plasma: Effect of uncertainties in the plasma chemistry

Antonin Berthelot and Annemie Bogaerts

Department of Chemistry, Research group PLASMANT, University of Antwerp, Universiteitsplein 1, 2610 Antwerp, Belgium

E-mail: antonin.berthelot@uantwerpen.be

Abstract. Low-temperature plasma chemical kinetic models are particularly important to the plasma community. These models typically require dozens of inputs, especially rate coefficients. The latter are not always precisely known and it is not surprising that the error on the rate coefficient data can propagate to the model output. In this paper, we present a model that uses N=400 different combinations of rate coefficients based on the uncertainty attributed to each rate coefficient, giving a good estimation of the uncertainty on the model output due to the rate coefficients. We demonstrate that the uncertainty varies a lot with the conditions and the type of output. Relatively low uncertainties (about 15 %) are found for electron density and temperature, while the uncertainty can reach more than an order of magnitude for the population of the vibrational levels in some cases and it can rise up to 100 % for the CO_2 conversion. The reactions that are mostly responsible for the largest uncertainties are identified. We show that the conditions of pressure, gas temperature and power density have a great effect on the uncertainty and on which reactions lead to this uncertainty. In all the cases tested here, while the absolute values may suffer from large uncertainties, the trends observed in previous modeling work are still valid. Finally, in accordance with the work of Turner, a number of "good practices" is recommended.

Keywords: CO_2 conversion, uncertainties, plasma chemistry, vibrational kinetics

Submitted to: *Plasma Sources Sci. Technol.*

1. Introduction

A large part of the energy consumed on Earth originates from fossil fuels, which has a detrimental effect on the climate. The idea of re-using the emitted CO_2 and transforming it into valuable chemicals has thus been gaining increasing interest in recent years [1]. One of the most common applications would be to dissociate CO_2 into CO, which can then be used to synthesize fuels.

It was shown that low-temperature plasmas can be an energy-efficient way to dissociate CO_2, and in particular microwave discharges and gliding arc discharges [2, 3]. Indeed, non-equilibrium cold plasmas have the interesting properties to exhibit

a much larger electron temperature than gas temperature, enabling the possibility for endothermic reactions to occur at relatively low gas temperature.

Therefore, in recent years, a lot of efforts have been made to obtain more insight in the CO_2 plasma, in order to improve the energy efficiency of the splitting process. Experimentally, different types of discharges have been studied, and the most common types are microwave (MW) plasmas [4, 5, 6, 7], gliding arc plasmas (GAP)[8, 9] and dielectic barrier discharges (DBD)[10, 11, 12].

It is reported that microwave and gliding arc plasmas offer much better energy efficiencies than DBDs. In these discharges, the electron temperature is usually in the range between 1 and 2 eV, which makes vibrational excitation one of the main electron energy loss channels. It is thus in theory possible to significantly enhance dissociation through a large vibrational excitation. This dissociation channel is usually considered to be the most energy-efficient one.

Reaching a large vibrational population is however not an easy task [13] and a better understanding of the plasma kinetics is needed to reach higher energy efficiencies. Kinetic modeling is therefore a powerful tool that gives insights in the processes occurring in the plasma which are typically not accessible experimentally. Pietanza and colleagues from the University of Bari [14, 15, 16, 17, 18, 19] focused on the coupling between the plasma kinetics and the electron energy distribution function (EEDF) and the different dissociation mechanisms, while in our group at the University of Antwerp, we focused mainly on the determination of the vibrational distribution, the improvement of the conversion and energy efficiency, the plasma chemistry and the physics of the discharge [13, 20, 21, 22, 23, 24, 25, 26, 27, 28].

Furthermore, Ponduri et al. [29] developed a time-dependent 1D model to describe the conversion of CO_2 in a DBD. Janeco et al [30] focused on the electron kinetics in a $He/CH_4/CO_2$ discharge to understand the role of He. Grofulović et al. [31] proposed a set of cross sections for CO_2 plasmas by comparing swarm parameters to the results of a two-term Boltzmann solver and the available experimental data. In particular, they recommended, along with Bogaerts et al. [25], to use the Phelps 7eV excitation cross section [32] as a dissociation cross section, which we use in this work. Koelman et al. [33] performed a first step toward the verification of the rate coefficient data and compared the results of two different global models using the same chemistry set.

One of the main issues encountered when developing such a model is the reliability of the rate coefficients and cross sections used. This issue was first brought to the attention of the plasma community by M. Turner [34, 35, 36] for a helium-oxygen mixture. The large uncertainty that exists on some of the rate coefficients leads to an uncertainty on the modeling results, which hinders their predictive capacities. Moreover, most papers refer to other papers using the rate coefficients cited in these papers and they do not refer to (or check) the original references where the expressions for these coefficients were determined. This leads to an increase in the chance of making a copy error.

The aim of this work is to find the original source of the rate coefficients that we use in our CO_2 kinetics model and to understand how the uncertainty on the input rate

coefficients and cross sections leads to uncertainties on the model output, thus giving an idea on the reliability of the model, both qualitatively and quantitatively, following the method proposed by M. Turner[34]. A statistical treatment of the data is used to pinpoint which rate coefficient has most effect on different outputs. This work should be seen as a first step towards building a more reliable database for CO_2 plasma kinetics. It stands as the continuation of the work initiated by Koelman et al [33].

This paper is organized as follows. In part 2, we first describe the model, and the conditions used in the model (in part 2.1). We then introduce the chemistry set (in part 2.2). In part 2.3, we explain the procedure used to determine the uncertainty on the output and in part 2.4, we explain the statistical treatment used to treat the data. The results are presented in part 3. This part contains two subparts. In part 3.1 we show the uncertainty on different model outputs (electron temperature and density, vibrational distribution function of the asymmetric stretch mode of CO_2 and CO_2 conversion) for different conditions. In part 3.2, we illustrate which rate coefficients are mainly responsible for the uncertainty of the various model results and we give some recommendations for good practice in chemical kinetics modeling. Finally, conclusions are given in section 4.

2. Model description

2.1. Plasma model

A zero-dimensional chemical kinetics model using the code ZDPlasKin [37] is developed. The density of each of the plasma species n_s shown in table 1 below is calculated using:

$$\frac{dn_s}{dt} = \sum_j R_j[a_{sj}^R - a_{sj}^L] = \sum_j (k_j \prod_l n_l)[a_{sj}^R - a_{sj}^L] \quad (1)$$

The index j refers to reaction j and the index l refers to the different reactants of reaction j. a_{sj}^R and a_{sj}^L are the right- and left-hand side stochiometric coefficients of species s, respectively. R_j is the reaction rate of reaction j, k_j is its rate coefficient. The chemical kinetics part is coupled, within the ZDPlasKin framework, to the Boltzmann solver BOLSIG+[38]. The electron energy distribution function (EEDF) is calculated using the same set of cross sections used for the kinetic part (Table A1), including superelastic collisions. The electron mean energy is obtained from the EEDF, providing also the electron temperature. During the simulation, the EEDF is regularly updated to reflect the changing chemical composition due to CO_2 conversion into CO and O_2 and the change in the value of the reduced electric field. Namely, the EEDF is updated if the gas temperature or the electron density change more than 3%, or if the reduced electric field or the density of a species reacting with electrons change more than 0.1 %. Calculating the EEDF is computationally expensive and updating it more often would result in a much longer computational time, which this kind of study cannot afford.

The model starts with pure CO_2 and a Botzmann vibrational distribution function at t=0. A power deposition P_{dep} is applied until the Specific Energy Input (SEI) reaches

1 eV/molec and then drops to 0. The gas temperature T_g and the pressure p are kept constant and are considered as parameters in this study. The power density is taken proportional to the pressure, as in our previous work [13]. This is done to ensure that the ratio between power density and pressure is constant, so that the data is comparable over different pressures. Naturally, we expect the situation in reality to be more complex.

The plasma-on time can be defined as:

$$\tau = \frac{e}{k_B}\frac{p}{P_{dep}T_g} \times 1[eV/molec] \tag{2}$$

where k_B is the Boltzmann constant and e is the elementary charge, used to convert eV to J. Since P_{dep} is chosen proportional to the pressure p in all cases, τ does not depend on the pressure.

The CO_2 conversion is calculated following:

$$X(t)(\%) = \frac{n_{CO}(t)}{n_0 - \frac{1}{2}n_{CO}(t)} \tag{3}$$

where $n_{CO}(t)$ is the total CO density (all CO species) at a time t and $n_0 = \frac{p}{k_B T_g}$ is the initial CO_2 density. The second part of the denominator originates from the gas expansion. Since the model considers an isobaric process, the volume is not fixed and this needs to be taken into account when calculating the conversion.

2.2. Chemistry set

The chemistry set used in this work contains the species listed in Table 1. It is important to note that this chemistry set has been reduced compared to our previous work [13, 21, 22, 25], based on our previous chemistry reduction [27]. This simplification of the chemistry set is justified by the fact that some species only have a minor contribution to the outcome of the model. Therefore, they do not bring additional important information, given the uncertainty existing on the different outputs of the model (see results), while making the task of retrieving all the original sources much more complex. More generally, we would like to point out that adding more complexity in the plasma kinetic models does not necessarily give a better outcome of the simulation, since the chemistry of the more rare species is usually poorly known. Moreover, although included to some extent, the chemistry of CO and O_2 is described in less detail in this model than the chemistry of CO_2, which is justified because of the low CO_2 conversion at the conditions under study. A more detailed description of these species might be needed at conditions where these species are present in higher densities (i.e. higher CO_2 conversion).

The energy of the CO_2 levels is calculated using equation 4, as in [39, 21]:

$$E_{CO_2} = \sum_i \omega_i(v_i + \frac{d_i}{2}) + \sum_{j\geq i} x_{ij}(v_i + \frac{d_i}{2})(v_j + \frac{d_j}{2}) + x_{l_2l_2}l_2^2 \tag{4}$$

where ω_i, x_{ij} and $x_{l_2l_2}$ are spectroscopic constants determined by experiment and $d_i = (d_1\ d_2\ d_3) = (1\ 2\ 1)$ are the degeneracies of the three modes of vibration. We use

Table 1. Species described in the model.

Neutral ground states
CO_2, CO, O_2, O, C

Charged species
CO_2^+, CO^+, CO_4^+, O^-, O_2^-, CO_3^-, CO_4^-, e^-

Excited states	Associated energy [eV]	State[a]
$O_2[v_{1-4}]$	Anharmonic oscillator	
$CO[v_{1-10}]$	Anharmonic oscillator	
$CO_2[v_{1-21}]$	Anharmonic oscillator	(00n)
$CO_2[v_a]$	0.083	(010)
$CO_2[v_b]$	0.167	(020) + (100)
$CO_2[v_c]$	0.252	(030) + (110)
$CO_2[v_d]$	0.339	(040) + (120) + (200)
$CO_2[e_1]$	10.5	$(^1\Sigma_u^+)$ + $(^3\Pi_u)$ + $(^1\Pi_u)$
$O_2[e_1]$	0.98	$(a^1\Delta_g)$ + $(b^1\Sigma_g^+)$
$O_2[e_2]$	8.4	$(B^3\Sigma_u^-)$ + higher triplet states
$CO[e_1]$	6.22	$(a^3\Pi_r)$
$CO[e_2]$	7.9	$(A^1\Pi)$
$CO[e_3]$	13.5	$(a'^3\Sigma^+)$ + $(d^3\Delta_i)$ + $(e^3\Sigma^-)$ + $(b^3\Sigma^+)$
$CO[e_4]$	10.01	$(C^1\Sigma^+)$ + $(E^1\Pi)$ + $(B^1\Sigma^+)$ + $(I^1\Sigma^-)$ + $(D^1\Delta)$

[a] CO_2 electronic states designation from Grofulović et al.[31], O_2 and CO electronic states notation from Huber & Herzberg [42].

the following values[39]: ω_1 = 1354.31 cm^{-1}, ω_2 = 672.85 cm^{-1}, ω_3 = 2396.32 cm^{-1}, x_{11} = -2.93 cm^{-1}, x_{12} = -4.61 cm^{-1}, x_{13} = -19.82 cm^{-1}, x_{22} = 1.35 cm^{-1}, x_{23} = -12.31 cm^{-1}, x_{33} = -12.47 cm^{-1}, $x_{l_2l_2}$ = -0.97 cm^{-1}.

The energies of the CO vibrational levels are calculated using an anharmonic oscillator formula[40]:

$$E = \omega_e(v + 0.5) - \omega_e x_e(v + 0.5)^2 \quad (5)$$

v is the vibrational quantum number, ω_e = 2169.81 cm^{-1} and $x_e = 6.12 \times 10^{-3}$ is the anharmonicity coefficient[41]. The energies of the O_2 vibrational levels are taken from the Phelps database [32].

The list of the different reactions considered in this work in given in the Appendix A. Table A1 shows the electron impact reactions that use cross section data to retrieve the rate coefficients. Table A2 presents the electron impact reactions described by analytic expressions for the rate coefficients. Table A3 shows the list of reactions involving ions. Table A4 presents the reactions between neutral molecules, and finally table A5 lists

the reactions between the different vibrational levels. This research is performed in continuation of the work done in our group over the last few years. The procedure used to calculate the rate coefficients of the reactions involving vibrationally excited molecules is described in detail in Kozák et al.[21]

2.3. Uncertainty determination and computational procedure

Most experimentally derived expressions for the rate coefficients are given in the form of Arhenius expression 6.

$$k = AT_g^B exp(-E_a/k_B T_g) \tag{6}$$

where k is the rate coefficient, k_b is the Boltzmann constant, T_g the gas temperature. E_a the activation energy, and A and B are coefficients that are experimentally or theoretically determined. Note that reactions that involve electrons typically show an additional dependence to the electron temperature. One of the most important parts of this work was to retrieve the original source for each expression. We have done this as much as possible in order to estimate the uncertainty on the rate coefficients. Naturally, our choice of sources is also subject to errors and we invite the reader to form a critical opinion and to systematically check the primary source of the data.

The uncertainty can be considered to be contained in the parameter A, as long as the rate coefficient is used in the parameter range considered in the determination of the analytical expression, i.e. $\frac{\Delta k}{\overline{k}} = \frac{\Delta A}{\overline{A}}$, where ΔX refers to the uncertainty on a quantity X and $\overline{X}$ refers to its mean value.

The procedure used in this work is very similar to the initial work of M. Turner on this matter [34]. First, we assume that the probability of each rate coefficient for having a certain value can be derived from a log-normal distribution. As pointed out in [34], this choice is debatable as some of the extreme values for the rate coefficients may be non-physical. Nevertheless, we believe that it gives a good estimation of the uncertainty of the model and this study focuses on the different quantiles in the outcome of the simulations, in order to avoid these non-physical values. The probability $f(A_n = x_A; \Delta A, \overline{A})$ that the coefficient A in expression 6 has a value x_A, given its uncertainty ΔA, is given by a log-normal distribution [43]:

$$f(A_n = x_A; \Delta A, \overline{A}) = \frac{1}{x_A \sigma \sqrt{2\pi}} exp(-\frac{ln(x_A - \mu)^2}{2\sigma^2}) \tag{7}$$

where μ and σ are parameters that contain the mean value of A ($\overline{A}$) and the error ΔA:

$$\mu = ln(\frac{\overline{A}}{(\Delta A)^2 + \overline{A}^2}) \qquad \sigma = \sqrt{(ln(1 + (\frac{\Delta A}{\overline{A}})))} \tag{8}$$

Then, we create a large number (N=400) of different combinations of rate coefficients. Each rate coefficient k_n of a given combination n is chosen randomly based on the probability density described in equation 7. For rate coefficients k' that

are derived from another rate coefficient k (scaling laws), we multiply the scaled rate coefficient $\overline{k'}$ by a factor $\frac{k_n}{\overline{k}}$, i.e. $k'_n = \overline{k'}\frac{k_n}{\overline{k}}$ for each chemistry set n.

The model is ran using each combination of rate coefficients (i.e. 400 different inputs) and the different outcomes are compared, which gives an estimation on the error of the calculation results. An analysis of the correlation between the input value taken for a rate coefficient and a certain output gives us an indication of which reaction is important for this output.

It is important to note that only the uncertainty on the original rate coefficients is considered here. The uncertainty on the model results is in reality likely to be larger due to possible systematic errors, especially the error made when using the different scaling laws and the fact that not all vibrational states are considered in the model. The goal of this research is to understand how, and to which extent, the error on the rate coefficients propagates to the results of the model.

2.4. Statistical treatment

This study has two main goals: (i) to quantify the uncertainty on the modeling results due to the uncertainty on the rate coefficients and (ii) to identify the main sources of uncertainty.

For the first part, the results will be shown using different colors delimiting the different chosen quantiles. This illustrates the distribution of the data at any given abscissa. The median value will be presented by a black line.

When comparing different conditions, error bars have been drawn. They delimit the data within a confidence interval of 70 %, determined by the quantiles corresponding to the first 15 % and 85 % of the data (X_{15},X_{85}). For simplicity, we call the quantile delimiting the first p % of the data X_p in this study. The relative difference between upper and lower quantiles is also shown, as it gives a good estimation of the relative error for a given confidence interval (see 3.1). Note that the distribution of the data within the interval $[\overline{X}\text{-}\sigma_X,\overline{X}+\sigma_X]$ in a normal distribution, where σ_X is the standard deviation, is about 68 %. This explains our choice of a confidence interval of 70 %, although the distribution of the data is not symmetrical in our case.

For the second part of this study, the built-in Matlab® tools for correlations are used to rank which input is mostly correlated with which output. This information together with the uncertainty on the corresponding rate coefficients allows us to identify the main sources of uncertainty on a given output (see 3.2). In particular, the Spearman's ρ rank correlation coefficient is used [44]. It is the common linear correlation coefficient, using the rank variables instead of the variables themselves.

It measures how monotonic a particular model output f(x) is as a function of a model input x. It has the advantage, in comparison to a standard correlation coefficient, to also detect non-linear correlations. ρ varies between -1 and +1. A value of 0 means that there is no monotonic relationship between the input and the output. An absolute value of 1 means that the function f(x) is perfectly monotonic with x. The sign of ρ gives

information on whether the function is increasing (positive ρ) or decreasing (negative ρ). In this work, following several estimations, we considered that only an absolute value of ρ larger than 0.3 is significant.

3. Results and discussion

3.1. Quantification of the uncertainty on the plasma variables

As mentioned earlier, it is crucial for the reliability of a model to know the uncertainty on its output. These uncertainties can for sure hinder the quantitative predictive capacities of a model, but they might also have an influence on the qualitative predictions. This part aims at understanding the effect of the uncertainties of the rate coefficients on several outputs of our CO_2 0D chemical kinetics model, namely the electron temperature (Figure 1), the electron density (Figure 2), the vibrational distribution function (VDF, Figures 3 and 4) and the CO_2 conversion (Figures 5 and 6).

Showing the solutions of the model for the N=400 combinations of rate coefficients is obviously not desirable. Therefore, in Figures 1, 2, 3 and 5 we opted for a representation using different colors. Each color delimits a confidence interval. The confidence intervals of 90%, 70%, 50 % and 25 % are represented in yellow, orange, red and dark red, respectively. They correspond to the following intervals, respectively: [X_5,X_{95}], [X_{15},X_{85}], [X_{25},X_{75}], [$X_{37.5}$,$X_{62.5}$]. The black curve shows the median value.

Additionally, in order to quantify more precisely the dispersion of the data, we show the relative difference $(X_U - X_L)/X_{50}$ between the upper quantile X_U and the lower quantile X_L, using the right y-axis. The dotted line gives the relative difference for the interval [X_{15},X_{85}], hence a confidence interval of 70 %, while the dashed line gives the relative difference for the interval [$X_{37.5}$,$X_{62.5}$], hence a confidence interval of 25 %.

Since the uncertainty is typically condition-dependent, Figures 1, 2 and 5 show the results for four different conditions:

a) Basic case: 200 mbar, 200 W.cm^{-3}, 300 K, τ = 3.87 ms
b) Higher pressure: 1000 mbar, 1000 W.cm^{-3}, 300 K, τ = 3.87 ms
c) Higher power density: 200 mbar, 1000 W.cm^{-3}, 300 K, τ = 0.77 ms
d) Higher temperature: 200 mbar, 200 W.cm^{-3}, 2000 K, τ = 0.58 ms

The residence time τ varies upon the parameters chosen, as the latter is defined by the time needed to reach an SEI of 1eV/molec, cf equation 2. The letter of the different panels corresponds to the letters of this list. These conditions correspond to typical conditions encountered in microwave plasmas or in other types of discharges, and were used in our previous work as well [13].

More specifically, Figure 1 shows the electron temperature T_e for these four conditions. The end of the power pulse (τ) is indicated by the vertical dash-dot black line. At 300 K (Figure 1 a, b and c), T_e shows the same behavior: a very short and sharp increase at t = 0, followed by a decrease until approximately t = 0.1 ms (barely

visible in the figure) and a slower increase until a stable value is reached. T_e then drops almost immediately to 0 at the end of the power pulse. The uncertainty (defined as the relative difference between the values lying 35 % above or below the median value, i.e., a confidence interval of 70 %; see above) is here between 10 % (Figure 1 a, b) and 15 % (Figure 1 c) in the plasma (dotted line).

At 2000 K (Figure 1 d), the behavior is slightly different: T_e increases sharply at t = 0 and then decreases for about 0.1 ms. Then, it reaches a rather stable value around 1 eV until the end of the plasma. The uncertainty is lower, around 5% in the plasma.

It is important to note that while the error on the electron temperature may appear small, it can have a major effect on the electron impact rate coefficients, since they are particularly sensitive to the electron energy.

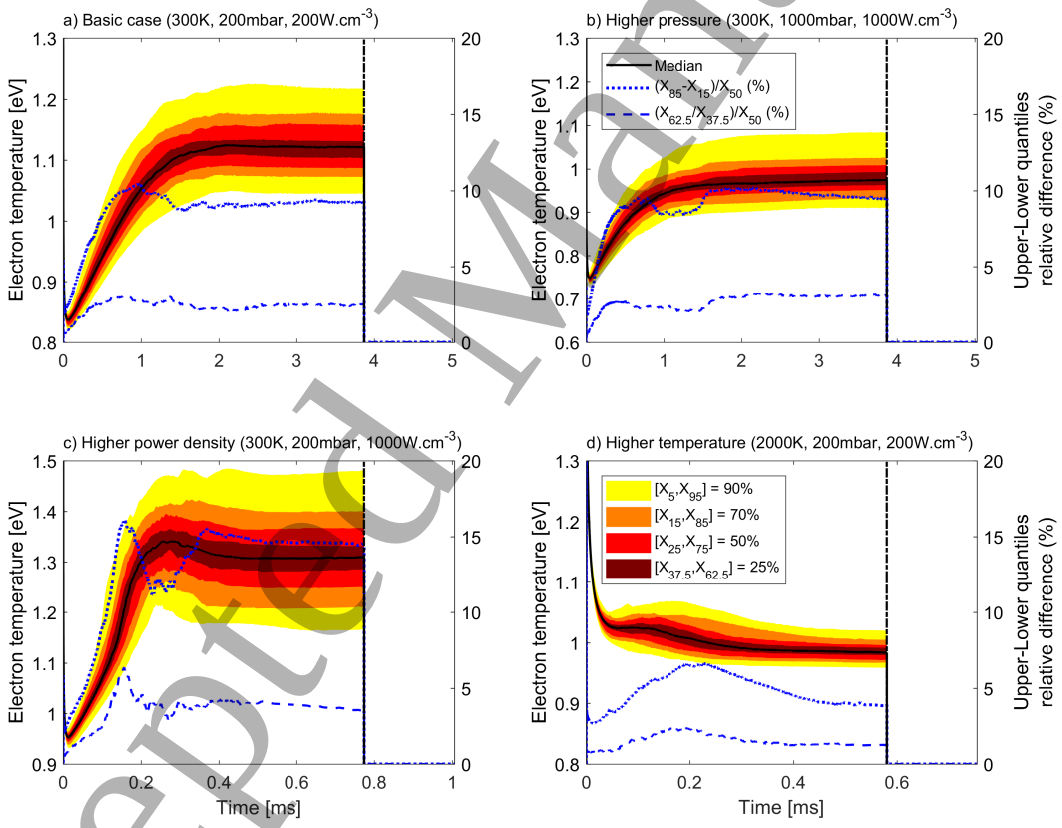

Figure 1. Electron temperature (left y-axis) as a function of time for four different cases. The different colors delimit different quantiles of the N = 400 solutions at each time. The median value is shown by the black curve. From lighter to darker, they correspond to 90%, 70%, 50% and 25% of the solutions. The end of the pulse is represented by the vertical dashed black line. The relative difference between the upper and the lower quantiles (right y-axis) are shown with the dotted blue line (corresponding to the orange zone; confidence interval of 70 %) and the dashed blue line (corresponding to the dark red zone; confidence interval of 25 %).

Figure 2 shows the calculated electron density n_e. The absolute value of the electron

density depends on the conditions. However, the four curves follow a similar trend: n_e rises quickly at the beginning of the power pulse and reaches a stable value after less than 0.1 ms. At the end of the power pulse, the electron density decreases exponentially. The error is typically 10 % or below in the plasma. In the afterglow, particularly in the beginning at 300 K, we see a sharp increase of the uncertainty, reaching up to 90 %. With decreasing electron density, the uncertainty decreases as well, to values ranging from 20 to 50 %. This sharp increase in the uncertainty is caused by the fact that a different choice of rate coefficients has a large effect on the decay time of the electron density. However, the electron density in the afterglow does not play a significant role in the CO_2 conversion at this relatively high pressure, so this uncertainly will be of minor importance to the overall uncertainty of the model. At 2000 K, the uncertainty remains rather low and increases from about 5 % to a bit more than 15 %.

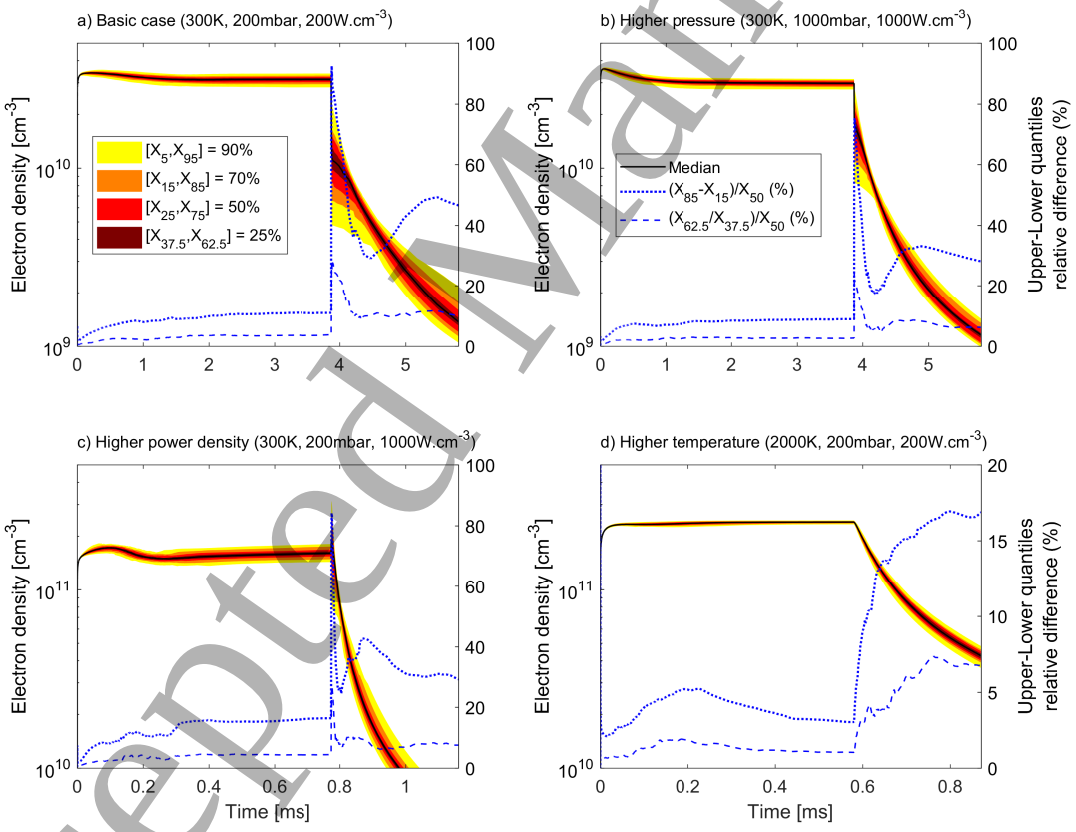

Figure 2. Electron density (left y-axis) as a function of time for four different cases. The different colors delimit different quantiles of the N = 400 solutions at each time. The median value is shown by the black curve. From lighter to darker, they correspond to 90%, 70%, 50% and 25% of the solutions. The relative difference between the upper and the lower quantiles (right y-axis) are shown with the dotted blue line (corresponding to the orange zone; confidence interval of 70 %) and the dashed blue line (corresponding to the dark red zone; confidence interval of 25 %).

Figure 3 shows the VDF at the beginning of the plasma (t = 0.1 ms, Figure 3a and

b) and at a later stage of the plasma (t = 2 ms in Figure 3c and t = 0.5 ms in Figure 3d). Only two conditions are presented here: the basic case (200 mbar, 200 W.cm^{-3}, 300 K, τ = 3.87 ms) and the higher temperature case (200 mbar, 200 W.cm^{-3}, 2000 K, τ = 0.58 ms). Indeed, the results at higher pressure or power density are similar to those of the basic case.

The typical non-equilibrium shape of the VDF described in our previous work [13] is present for the basic case (Figure 3 a and c), i.e. at low gas temperature. The increasing population of the vibrationally excited states over time is visible by comparing Figure 3a and Figure 3c. Using the population of the first asymmetric mode, we can associate a vibrational temperature to the VDF, giving an estimation of the extent of vibrational excitation. At t = 0.1 ms (Figure 3a), the vibrational temperature varies between 830 K and 978 K (for a confidence interval of 70 %), with a median value of 900 K (hence an uncertainty of 16 %). At t = 2 ms (Figure 3c), it varies between 1275 K and 1703 K (for the same confidence interval), with a median value of 1472 K (hence, an uncertainty of 29 %).

The uncertainty on the VDF also increases with time, ranging from 50 % to 300 % for the population of different energy levels at t = 0.1 ms and between 50 % and 1400 % at t = 2 ms. Indeed, the error on the densities on the vibrational levels builds up over time and there are no mechanisms that compensate this build-up, which explains the increase of the uncertainty. The uncertainty on the VDF is thus large and can reach more than an order of magnitude. This is expected since many reactions occur between the vibrational levels and they are particularly important in determining the VDF. Thus, a small error on the original VT and VV rates coefficients can have much larger consequences on the VDF.

On the other hand, at a temperature of 2000 K (Figure 3 b and d), the VDF stays rather constant and resembles a Boltzmann distribution. This behavior was also observed in our previous work and is attributed to the fast VT relaxation occurring at high gas temperature. The vibrational temperature is about 2000 K at all time, with no significant dispersion of the results. Since the large VT transfers bring the VDF back to a Boltzmann distribution, the uncertainty is here much lower. It ranges from 5 % to 45 % and does not really change over time.

Similarly, using the population of the 4 symmetric states, we can obtain a vibrational temperature for the symmetric states. At t = 0.1 ms and with a gas temperature of 300 K, a pressure of 200 mbar and a power density of 200 W.cm^{-3}, corresponding to the basic case, we obtain the following median temperatures for the vibrational symmetric mode levels v_a, v_b, v_c and v_d: $T_{va} = 320K$, $T_{vb} = 472K$, $T_{vc} = 565K$ and $T_{vd} = 519K$. Using a confidence interval of 70 %, the uncertainties are 10 %, 13 %, 12 % and 6 %, respectively. At t = 2 ms, the symmetric temperatures are $T_{va} = 1111K$, $T_{vb} = 1346K$, $T_{vc} = 1386K$ and $T_{vd} = 795K$. The uncertainties are 92 %, 67 %, 60 % and 22 %, respectively. Note that the vibrational energy of the symmetric levels is rather low. Their population is thus comparable to the ground state population, which explains the high sensitivity of their temperatures to the uncertainties of the rate

coefficients. At this high level of symmetric excitation, inter-mode energy exchanges can become important[45]. These non-linear effects are partly included in the model for the low-energy levels through reaction V5 (see Appendix A), but not for the higher energy levels, as this would lead to a complexity that is beyond this study.

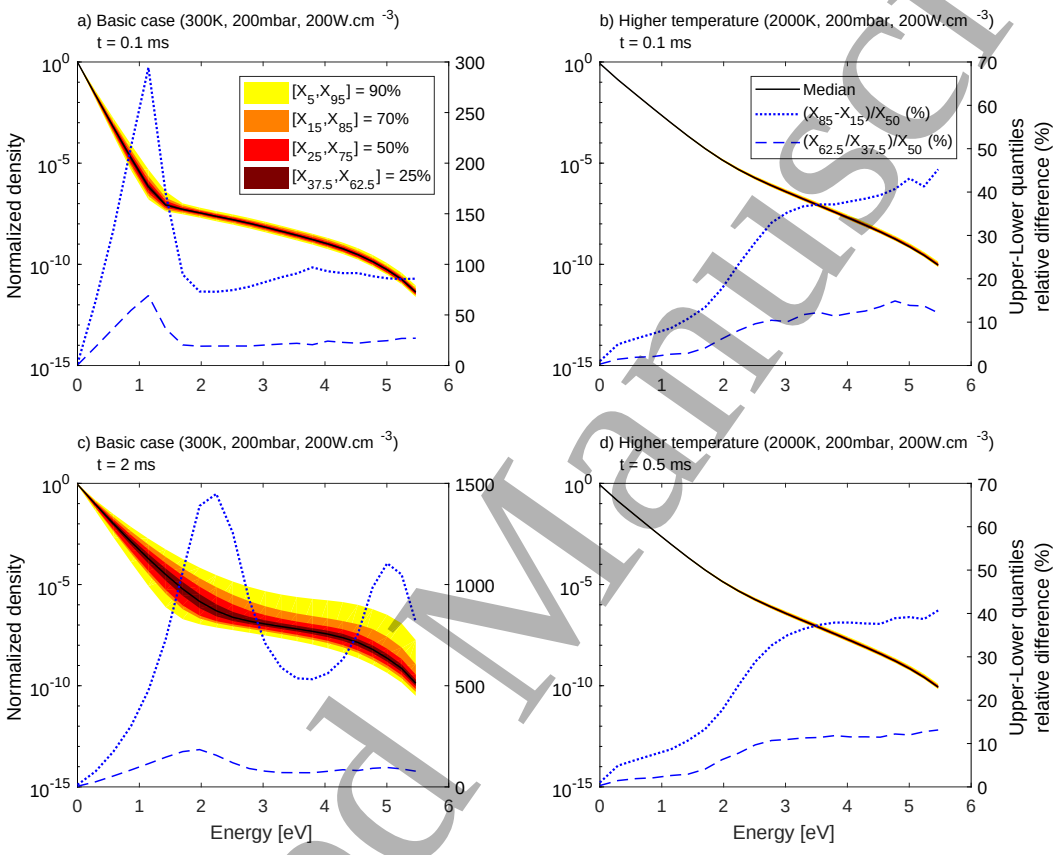

Figure 3. Vibrational distribution function (left y-axis) at the beginning of the power pulse (t = 0.1 ms, panels a and b) and at a later stage in the power pulse (t = 0.5 and 2 ms, panels d and c, respectively) for the basic case (panels a and c) and the higher temperature case (b and d). The median value is shown by the black curve. The different shades delimit different quantiles of the N = 400 solutions. From lighter to darker, they correspond to 90%, 70%, 50% and 25% of the solutions. The relative difference between the upper and the lower quantiles (right y-axis) are shown with the dotted blue line (corresponding to the orange zone; confidence interval of 70 %) and the dashed blue line (corresponding to the dark red zone; confidence interval of 25 %).

Thus, the uncertainty on the VDF depends a lot on the conditions, as seen in Figure 3. Given the magnitude of the uncertainty, one question then arises: to which extent are the trends observed in the calculations for different conditions still valid, keeping in mind the uncertainties? Figure 4 shows the vibrational distribution function for the four different conditions studied here at a time t = 0.1 ms (Figure 4a) and t = 0.5 ms (Figure 4b). Error bars are added, corresponding to a confidence interval of 70 %, i.e. delimiting the interval $[X_{15},X_{85}]$.

At t = 0.1 ms (Figure 4 a), we see that the high pressure case and the high gas temperature case exhibit a smaller uncertainty. Indeed, the VDF is then closer to equilibrium and is thus easier to predict. In typical experimental cases, because of the high gas temperature, extreme non-equilibrium conditions are very difficult to reach. On the other hand, for the basic case and particularly for the high power density case, the uncertainty can become very large, even at the beginning of the simulation. It is also interesting to note that in the high pressure case, the uncertainty is maximum for the highly excited vibrational levels.

Nevertheless, the trends observed in our previous work [13], namely that the importance of higher vibrational levels increases with power density and decreases with temperature and pressure, are still visible and the difference between the VDFs is still significant.

At t = 0.5 ms (Figure 4 b), the trends are still the same, although vibrational excitation has had time to build up, which is particularly visible on the curve showing the high power density case. It is especially interesting to see that the uncertainty increases for the basic case but is drastically reduced for the high power density case.

This can be explained by the fact that vibrational excitation (i.e., vibrational ladder climbing) is building up at t = 0.1 ms. There, the results are thus very sensitive to the chosen combination of rate coefficients and very large uncertainties can occur. However, once the vibrational ladder climbing has built up and has reached a sufficient population, the CO_2 molecules begin to dissociate very quickly, which seems to significantly reduce the uncertainty.

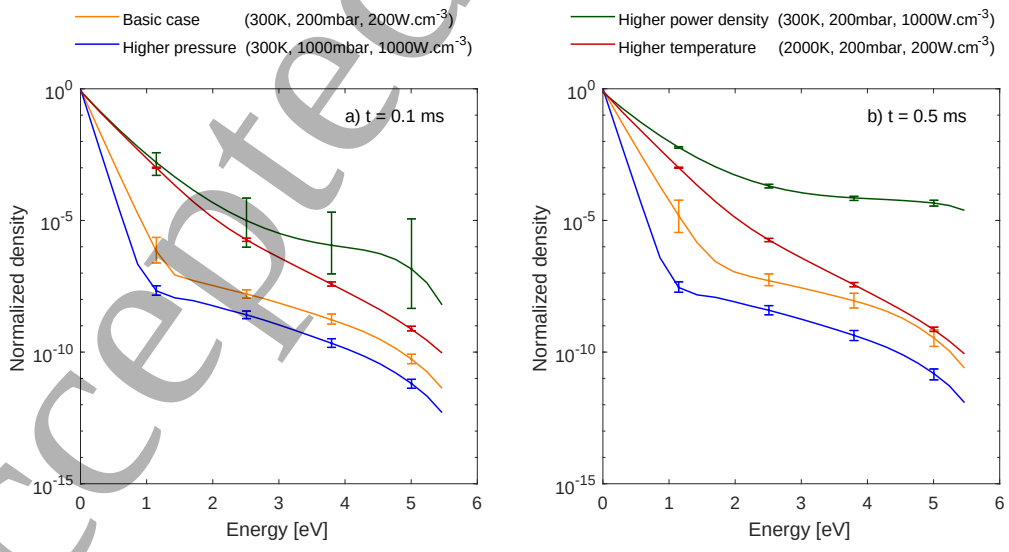

Figure 4. Median value of the vibrational distribution function at t = 0.1ms (panel a) and at t = 0.5 ms (panel b) for different conditions (see legend). The error bars delimit the interval $[X_{15},X_{85}]$, corresponding to a confidence interval of 70%.

Figure 5 shows the CO_2 conversion as a function of time for the four different

conditions listed above. The end of the power pulse is indicated by the vertical black dotted line. The trends are rather similar in all cases: the CO_2 conversion increases linearly inside the plasma and then stays constant, although it slowly increases in the 2000 K case (Figure 5 d). This slow increase at 2000 K is due to thermal conversion, that does not require plasma. Note that at low gas temperature (Figure 5 a, b and c), the conversion starts with a short delay after the beginning of the power pulse (at t = 0). This is particularly visible in Figure 5c, and it is due to the time that the vibrational levels require to be populated first, before they can give rise to conversion.

The uncertainty is quite large and relatively constant in Figure 5 a, b and d, between 70% and 110 %. In Figure 5 c, it reaches more than 250 % at the beginning of the conversion and then stabilizes at a bit more than 50%. This can be understood by knowing that most of the conversion originates from vibrationally excited CO_2 in this case. Since the build-up time of the vibrational population is not the same with all combinations of rate coefficients, as mentionned above, there is a delay between the beginning of the conversion from one simulation to the other. This means that simulations with practically zero conversion in the beginning are compared to simulations where the conversion is already non-negligible, causing a large uncertainty. Eventually, as we have seen in Figure 4 b, since the vibrational excitation becomes very large in the vast majority of the simulations, the conversion happens and the uncertainty reaches more reasonable values, although it is still quite large.

The different values of conversion, calculated long after the end of the plasma pulse, at t = 50 ms, are plotted as a function of pressure in Figure 6. In the basic case, as we have also seen in Figure 5, the conversion is very low: it drops from 1.4 % at 100 mbar to 0.5 % at 1000 mbar. The conversion in the high temperature case is around 0.7 %, independent from the pressure. The higher power density yields a much larger conversion at low pressure, reaching 8 % at 100 mbar, but decreasing to 0.5 % at 1000 mbar. The uncertainties are particularly important for low pressures and high power deposition, at low gas temperature.

These results indicate that there is a threshold of power density above which vibrationally-induced dissociation becomes important. This threshold depends on pressure and on gas temperature, as we have seen in our previous work [13]. Under this threshold, dissociation is either due to electron impact dissociation or to thermal processes and the non-equilibrium aspect of the plasma is not fully exploited. This also has an effect on the uncertainties: vibrationally-induced dissociation is a complex mechanism and an accurate prediction of its magnitude requires using multiple reactions. The most important reactions are vibrational-translational (VT) relaxations, vibrational-vibrational (VV) relaxations and electron-vibration energy transfers (e-V). Naturally, the uncertainty on all these reactions builds up on the final result. On the other hand, electron impact dissociation and thermal dissociation are the result of much simpler processes, which allows for more accurate predictions.

Note that the values of conversion appear to be low in comparison to experiments, especially in the basic and the high temperature case. It is worth mentioning that

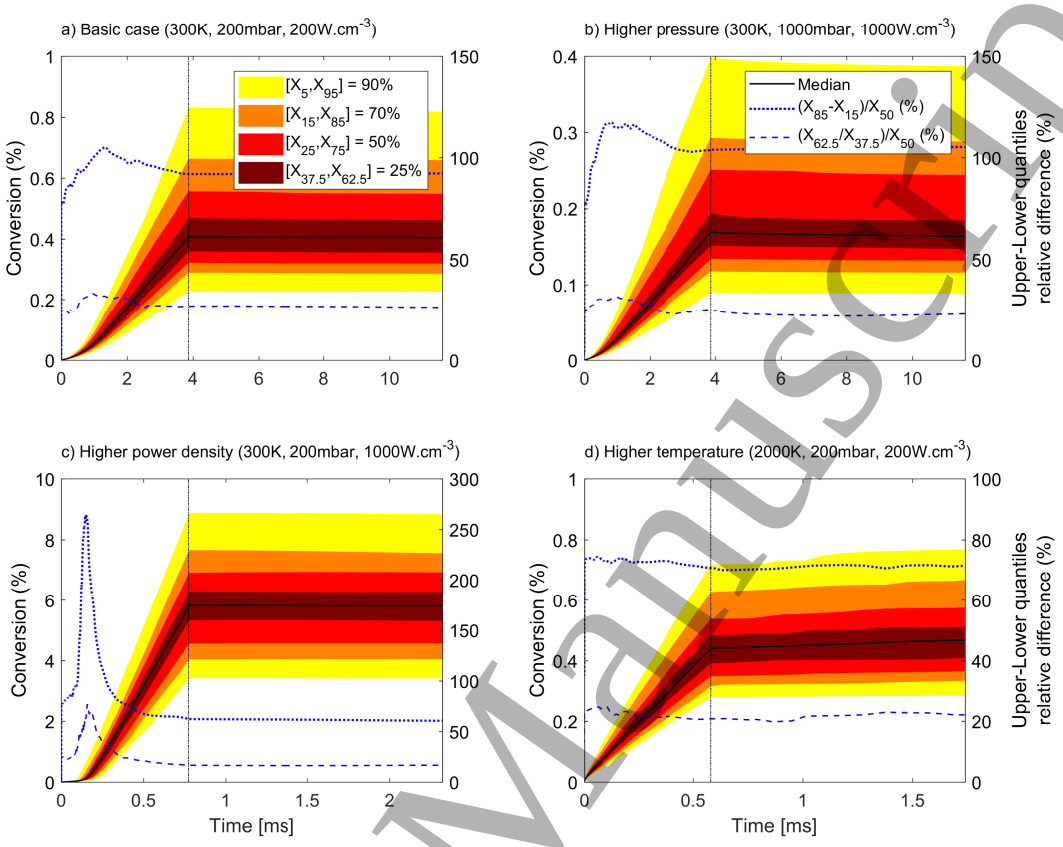

Figure 5. CO_2 conversion as a function of time for four different cases. The different colors delimit different quantiles of the N = 400 solutions at each time. The median value is shown by the black curve. From lighter to darker, they correspond to 90%, 70%, 50% and 25% of the solutions. The relative difference between the upper and the lower quantiles (right y-axis) are shown with the dotted blue line (corresponding to the orange zone) and the dashed blue line (corresponding to the orange zone; confidence interval of 70 %) and the dashed blue line (corresponding to the dark red zone; confidence interval of 25 %).

these test scenarios cannot be transposed to complex experimental cases, due to their simplicity. They are chosen to be simple in this study on the uncertainties of our CO_2 chemical kinetics model in order to be able to analyze the data and to understand the source of the uncertainties.

3.2. Correlations between uncertainties in the model results and responsible reactions

The aim of this part is to understand which reactions have a substantial effect on the results of the model. We focus here on the CO_2 conversion and the vibrational excitation, as they are very important for the application and they are characterized by the largest uncertainties, as seen in part 3.1 above. Indeed, for those calculation results with lower uncertainties, like the electron temperature and density, it was found difficult to draw meaningful conclusions about the effect of specific reactions.

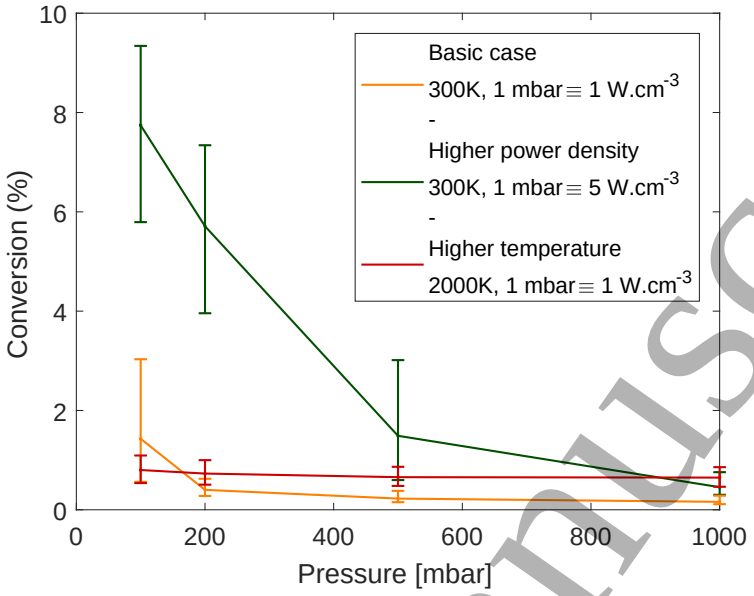

Figure 6. Calculated conversion as a function of pressure for different conditions: two different gas temperature, $T_g = 300K$ (yellow and green curve) and $T_g = 2000K$ (red curve); two different power depositions, low (orange and red curves) and high (green curve). The error bars delimit the interval [X_{15},X_{85}], corresponding to a confidence interval of 70%. The conversion is calculated at t=50ms.

To grasp the concept of the Spearman's rank correlation coefficient described in part 2.4, Figure 7 shows the values of the calculated CO_2 conversion as a function of the relative value of the rate coefficient for electron impact excitation to the asymmetric mode vibrational levels (any of the levels), for two conditions: the basic case (Figure 7 a) and the high power density case (Figure 7 b). The same data was used in Figure 6: each scatter plot in Figure 7 corresponds to one conversion data point and error bar in Figure 6.

The Spearman's ρ coefficient is calculated to be 0.15 and 0.69, in the basic and the high power density case, respectively. Indeed, Figure 7 shows that the correlation between the calculated CO_2 conversion and the rate coefficient for vibrational excitation is obvious in the high power density case, while no trend stands out in the basic case.

This information is summarized, and extended also to other reactions, in Figure 8, which shows the Sperman's ρ coefficient for the four conditions indicated, between the CO_2 conversion and the rate coefficients of seven important reactions. The other rate coefficients did not show any noticeable trend (i.e. $\rho < 0.3$). The results for the basic case and the higher pressure case are similar. In both cases, electron impact dissociation (X4) is, by far, the main source of uncertainty. Reaction (I9), i.e. a formation process of CO_2 upon collision of a negative ion with O atoms, is the second source of uncertainty. Indeed, since electron impact dissociation is the main dissociation mechanism at these conditions, the ion kinetics, which is strongly related to the electron kinetics, is also important. No other significant correlations were found.

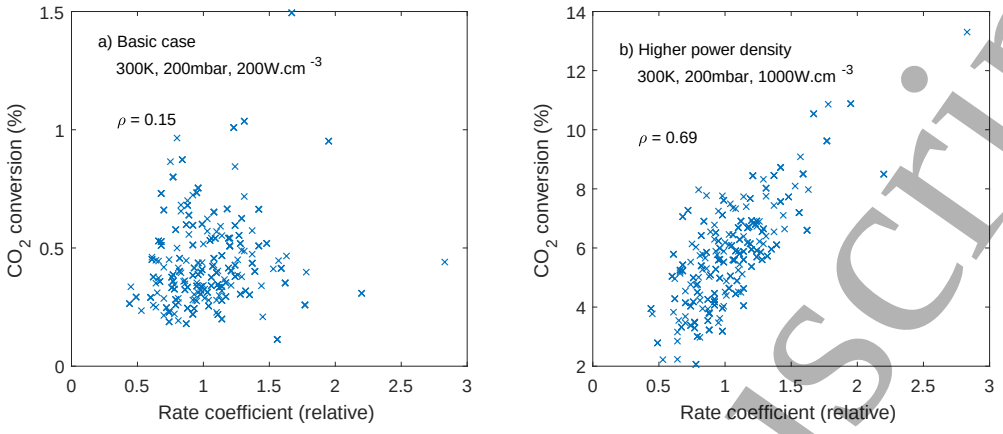

Figure 7. Scatter plot of the CO_2 conversion calculated at t=50ms as a function of the relative rate coefficient for electron impact vibrational excitation to the asymmetric mode levels, i.e. $k_n/\overline{k}$ for two different conditions (a: basic case - b: high power density case). In each panel, each of the N=400 points corresponds to a simulation made with a different choice of rate coefficients. The Spearman's ρ correlation coefficient is indicated in both cases.

At higher temperature, electron impact dissociation (X4) is still the main source of uncertainty, followed by CO_2 dissociation upon O atom impact (N2). Kozák and Bogaerts[22] also reported that modifying the activation energy of this reaction has a large effect on the conversion. The uncertainty on this rate coefficient is large, causing a large effect on the CO_2 conversion.

At higher power density, more reactions were found to be significant. The main correlation was found with electron impact asymmetric mode vibrational excitation (X7) (also shown in Figure 7 b), followed by electron impact symmetric mode vibrational excitation to CO_2v_a and CO_2v_b, (X6a) and (X6b), respectively. Increasing the rate coefficient of reaction (X4), (N2) and (X7) has a beneficial effect on the conversion. The correlation coefficient for the other rate coefficients is too low (< 0.3) to draw reliable conclusions about their effect on the CO_2 conversion

It is also found that increasing the VT reaction rate coefficient (V1) has a detrimental effect on the CO_2 conversion in the high power density case. These trends correspond to our previous observations, showing that at higher power density, the dissociation mainly originates from vibrationally excited levels. Therefore, the main source of uncertainty arises from the reactions that are needed to obtain the VDF.

Figure 9 shows the obtained Sperman's ρ coefficient for the four conditions indicated between the density of one of the highest asymmetric mode vibrational levels of CO_2, i.e. CO_2v_{20}, and the rate coefficients that are found to yield the most significant correlations. Figure 9a considers the CO_2v_{20} density at t = 0.1 ms while Figure 9 b shows the CO_2v_{20} density at t = 0.5 ms, corresponding to Figure 4a and b, respectively.

This particular asymmetric mode vibrational level was chosen since its determination leads to a large uncertainty, particularly in the high power density case

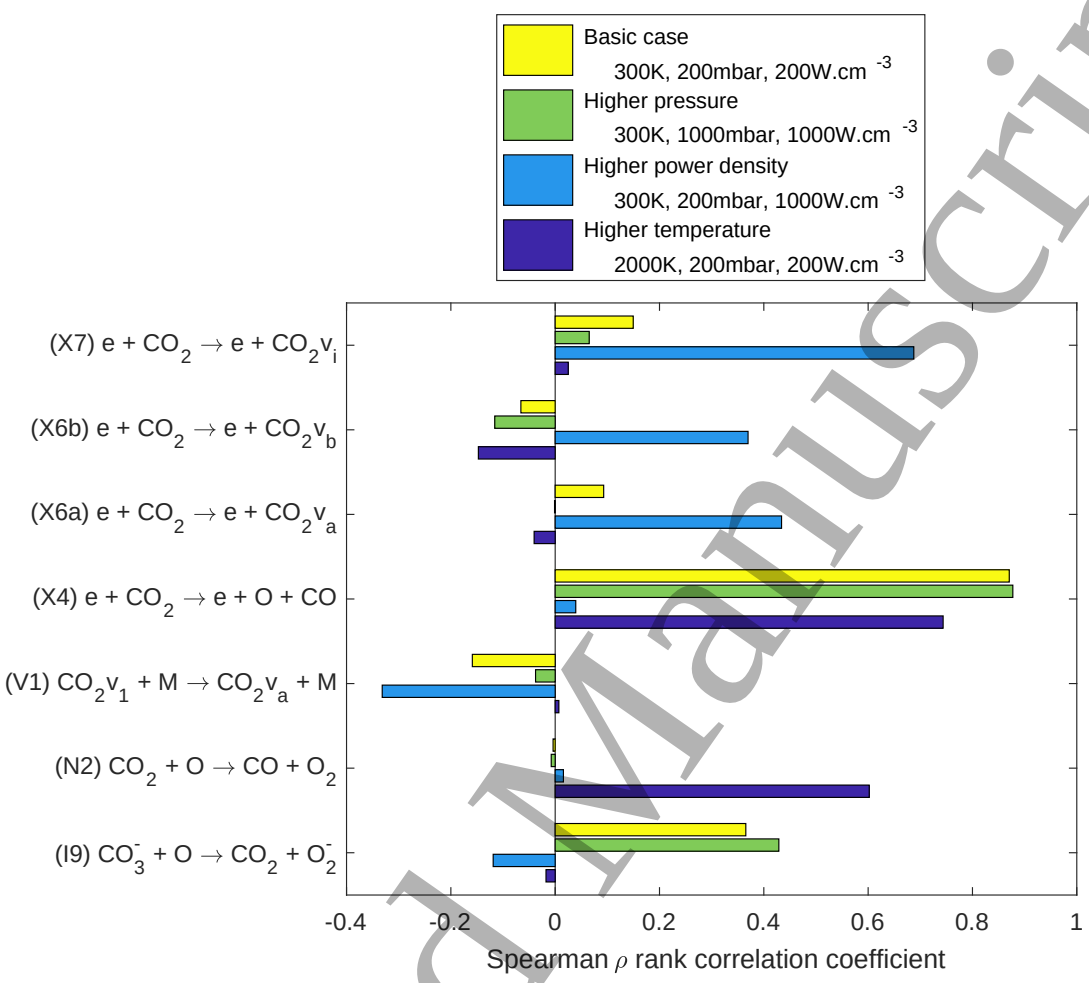

Figure 8. Spearman's ρ rank correlation coefficient between the calculated CO_2 conversion at t=50ms and the rate coefficients of different reactions for four different conditions (see legend). The coefficients are only shown when the CO_2 conversion exhibits a clear dependence on the rate coefficient of that reaction, i.e. if $\rho > 0.3$ for one of the conditions.

at t = 0.1 ms, as observed in Figure 4a.

At t = 0.1 ms (Figure 9a), the basic case, the higher pressure case and the higher power density case show similar correlations. The main source of uncertainty is found to be reaction (X7), i.e., electron impact vibrational excitation. Increasing the rate coefficient of this reaction clearly enhances the density of CO_2v_{20}, which is logical. The VT relaxation reaction (V5) comes second, with a negative ρ coefficient, which is again logical. At higher temperature, X7 has again the main influence, but some more reactions play a role. Reactions N1, V1 and V2b show a similar negative correlation coefficient and X6c is found to have a clear positive correlation. The influence of N1 at higher temperature can be easily understood: for a highly excited level, the activation energy of dissociation reactions is lowered. Therefore, the activation energy of CO_2v_{20} is similar to the (relatively high) gas temperature, leading to a very high probability of

dissociation by reaction N1.

At t = 0.5 ms (Figure 9b), similar correlations are observed for the basic and the high pressure case, although V1 seems to be more important than at t = 0.1 ms. The correlations for the high power density case are quite different from what we have seen above. N2 is now the main depopulating mechanism, followed by V1. The influence of X7 is lower here. At 2000 K, the observations made in Figure 9a are still valid. Indeed, at 2000 K, the VDF thermalizes very quickly and thus, there is no important change in the kinetics between the beginning and the end of the plasma.

To summarize our results, we see that the uncertainty on the model results clearly depends on the conditions and the type of output. Knowing the magnitude of the uncertainties is necessary for a valid interpretation of the modeling results. This study shows that the absolute values predicted by the model are subject to quite large uncertainties. The CO_2 conversion and vibrational excitation have been identified as particularly sensitive to the uncertainties on the rate coefficients. This is perfectly understandable since obtaining these values requires to calculate several other quantities, which are themselves subject to uncertainties. In other terms, these "final" outputs combine all the uncertainties from the other quantities.

Despite these findings, it is important to note that the trends observed in our previous work [21, 22, 13] are still found back in the current study, accounting for the uncertainties. Given the complexity of the kinetics, this is a rather positive message. Indeed, when analyzing the results of a kinetic model, especially the more complex ones, one should be aware that the absolute values are subject to large uncertainties and the predictive power of such models is thus hindered. However, the trends that are predicted by the models seem to be valid and also contain very useful information.

Note that, as mentioned earlier, this study is only a first step in the direction of the Verification and Validation (V&V) of the kinetic modeling results, which was described by Turner [36]. Naturally, the rate coefficients are not the only source of uncertainty in the model and more systematic errors may be present, such as the influence of the different scaling laws that are used. Errors in the code may also still be present, despite our best efforts to ensure that there are none.

In accordance with Turner, we recommend a (non-exhaustive) number of 'good practices' that should be adopted by the low-temperature plasma modeling community. First, and probably most importantly, the original source of the rate coefficient data should be cited as much as possible, along with mentioning the uncertainty of the data. We have tried to do this as much as possible in this work, although it is sometimes not possible to access the original sources. Second, a large database of verified rate coefficients would be particularly useful for the plasma modeling community. These databases exist in other fields, such as the UMIST database [46] for astrophysics or the NIST chemistry webbook [47] to some extent. This work is started in the plasma community by LxCat [48], which is an extensive database of electron and ion scattering cross sections, swarm parameters, etc. Third, this type of study is highly necessary so that the modeling results can be analyzed in light of the uncertainties that exist.

Note that the calculation time might be a problem in more complex cases here, since the model needs to run for several hundreds of combination of rate coefficients, instead of just one. Finally, when possible, we would recommend a more systematic attempt to validate the modeling results and the chosen rate coefficients against experimental values, particularly species and electron densities, in a rigorous manner. In order to validate the rate coefficients over a wider range of parameters, it would be beneficial to control parameters, such as the gas temperature and the reduced electric field, in these experiments. Thus, the experiments should be carried out in a simple design, like a glow discharge with parallel electrodes, not optimized for CO_2 conversion studies in terms of conversion or energy efficiency, but for controlled experiments. Moreover, using various conditions in these experiments would allow to benchmark (or discard) different rate coefficients at these different conditions, since the dominant mechanisms depend on the conditions considered.

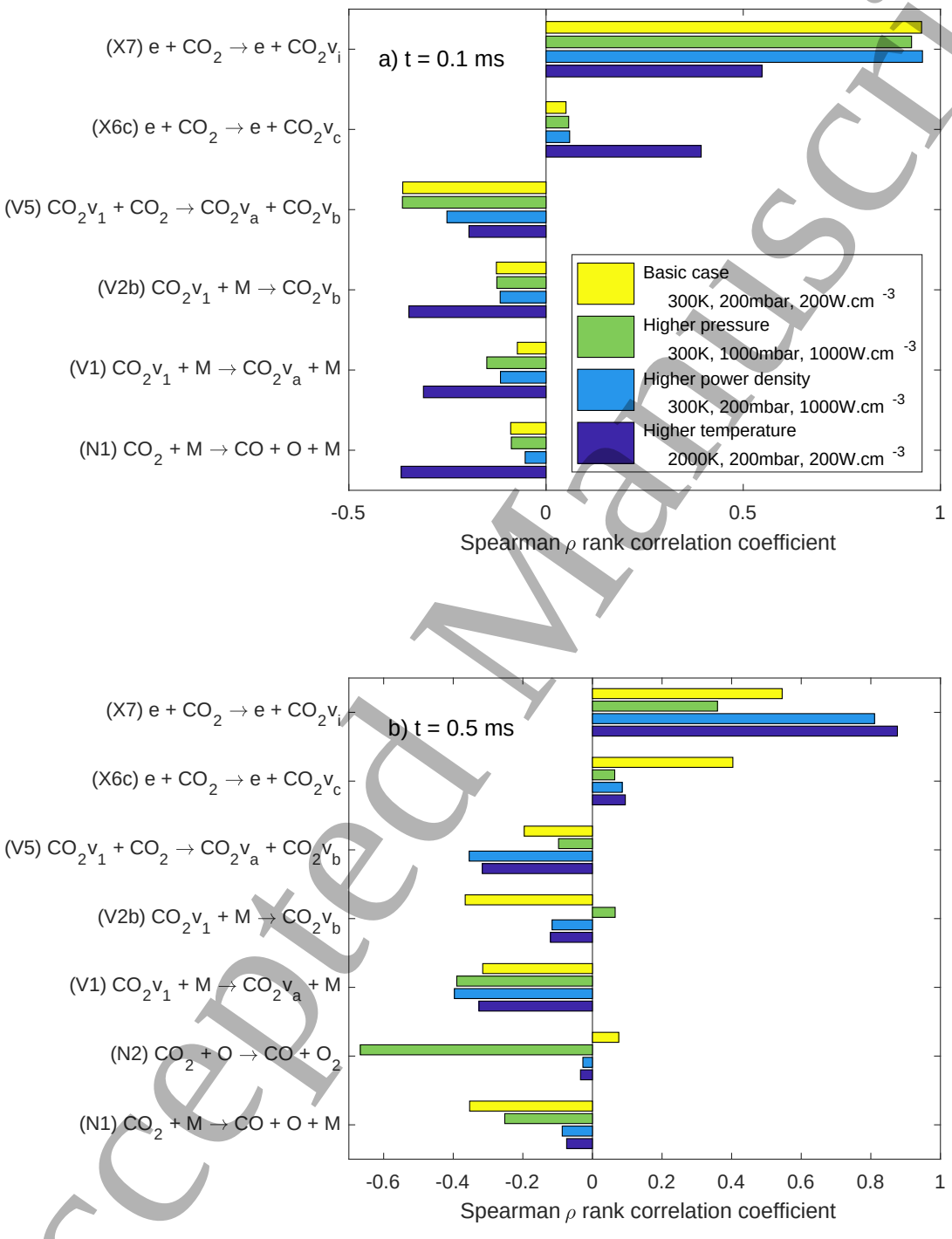

Figure 9. Spearman's ρ rank correlation coefficients between the calculated CO_2v_{20} density and the rate coefficients of different reactions for different conditions (see legend) at t = 0.1 ms (panel a) and at t = 0.5 ms (panel b). The coefficients are only shown when the CO_2v_{20} density exhibits a clear dependence on the rate coefficient of the reaction, i.e. if $\rho > 0.3$ for one of the conditions.

4. Conclusion

We have developed a zero-dimensional chemical kinetics model to describe the CO_2 conversion in a low-temperature plasma. A detailed description of the vibrational kinetics of CO_2, O_2 and CO is included. Using the uncertainty on the rate coefficients, which is typically in the order of 10-30 %, but can rise up to 100 % or even 200 %, a probability distribution was calculated for the rate coefficient of each reaction. Based on these probability distributions, 400 different combinations of rate coefficients have been created and used in the model for different conditions of pressure, power density and gas temperature to predict the uncertainty on the calculation results of the model. This method indeed shows how the uncertainty present on the rate coefficients propagates to the final results.

The electron density and electron temperature show relatively small errors, in the range of 15 % inside the plasma. The error on the electron density in the afterglow is more important, reaching up to 90 %, but will not be very critical due to the lower values of the electron density. The error on the population of the vibrational levels is much larger, reaching up to two orders of magnitude. This error is smaller when increasing the gas temperature and/or the pressure, i.e. conditions closer to equilibrium. The CO_2 conversion is also strongly affected by the uncertainties, whith errors ranging between 50 % and 110 % depending on the conditions.

By analyzing the correlations between the model results and the rate coefficients of the individual reactions, we can reveal which reactions contribute most to the uncertainty in the model results. Typically, the results that are sensitive to other calculated quantities, such as the VDF and the CO_2 conversion, seem to be particularly subject to uncertainties, since they combine all the uncertainties of the quantities needed to calculate them. The reactions can contribute most to the uncertainty in the VDF are the electron impact asymmetric mode excitation and the VV and VT reactions. Electron impact dissociation contributes most to the uncertainty in the CO_2 conversion, except in cases with strong vibrational excitation, where the reactions contributing to the uncertainty on the VDF also contribute to the uncertainty on the CO_2 conversion.

Finally, we recommend a number of "good practices" to improve the reliability of plasma kinetic modeling, in line with earlier recommendations by Turner[36]. Probably the most important is to systematically refer to the original sources of the data used. Creating a large database of verified rate coefficients would largely contribute to the improvement of the reliability as well. Validating the results of kinetic modeling using a certain series of rate coefficients against experiments would also be of great help for the community.

These aspects should be borne in mind when analyzing the calculation results of a chemical kinetics model. The main message emerging from this study is that the absolute value of certain model outputs has to be interpreted with caution. However, the trends still seem to be valid in the majority of the cases, and they also contain very useful information. Therefore, in the absence of certainty over the rate coefficients,

kinetic modeling should focus more on trends and the model results should be evaluated critically, both by the researchers and the readers.

5. Acknowledgement

We acknowledge financial support from the European Union's Seventh Framework Program for research, technological development and demonstration under grant agreement n° 606889. The calculations were carried out using the Turing HPC infrastructure at the CalcUA core facility of the Universiteit Antwerpen (UA), a division of the Flemish Supercomputer Center VSC, funded by the Hercules Foundation, the Flemish Government (department EWI) and the UA.

6. References

[1] J. A. Martens, A. Bogaerts, N. De Kimpe, P. A. Jacobs, G. B. Marin, K. Rabaey, M. Saeys, and S. Verhelst, "The Chemical Route to a Carbon Dioxide Neutral World," *ChemSusChem*, vol. 10, pp. 1039–1055, mar 2017.

[2] A. Fridman, *Plasma chemistry*. New York: Cambridge University Press, 2008.

[3] R. Snoeckx and A. Bogaerts, "Plasma technology – a novel solution for CO_2 conversion?," *Chemical Society Reviews, Under review*, 2017.

[4] R. I. Asisov, A. K. Vakar, V. K. Jivotov, M. F. Krotov, O. A. Zinoviev, B. V. Potapkin, A. A. Rusanov, V. D. Rusanov, and A. A. Fridman, "Non-equilibrium plasma-chemical process of CO_2 decomposition in a supersonic microwave discharge," *Proceedings of the USSR Academy of Sciences*, vol. 271, no. 1, 1983.

[5] T. Silva, N. Britun, T. Godfroid, and R. Snyders, "Optical characterization of a microwave pulsed discharge used for dissociation of CO_2," *Plasma Sources Science and Technology*, vol. 23, p. 025009, apr 2014.

[6] W. Bongers, H. Bouwmeester, B. Wolf, F. Peeters, S. Welzel, D. van den Bekerom, N. den Harder, A. Goede, M. Graswinckel, P. W. Groen, J. Kopecki, M. Leins, G. van Rooij, A. Schulz, M. Walker, and R. van de Sanden, "Plasma-driven dissociation of CO_2 for fuel synthesis," *Plasma Processes and Polymers*, no. July, pp. 1–8, 2016.

[7] N. den Harder, D. C. M. van den Bekerom, R. S. Al, M. F. Graswinckel, J. M. Palomares, F. J. J. Peeters, S. Ponduri, T. Minea, W. A. Bongers, M. C. M. van de Sanden, and G. J. van Rooij, "Homogeneous CO_2 conversion by microwave plasma: Wave propagation and diagnostics," *Plasma Processes and Polymers*, no. July, pp. 1–24, 2016.

[8] A. Indarto, D. R. Yang, J. W. Choi, H. Lee, and H. K. Song, "Gliding arc plasma processing of CO_2 conversion," *Journal of Hazardous Materials*, vol. 146, no. 1-2, pp. 309–315, 2007.

[9] T. Nunnally, K. Gutsol, A. Rabinovich, A. Fridman, A. Gutsol, and A. Kemoun, "Dissociation of CO_2 in a low current gliding arc plasmatron," *Journal of Physics D: Applied Physics*, vol. 44, p. 274009, jul 2011.

[10] D. Mei, X. Zhu, Y.-L. He, J. D. Yan, and X. Tu, "Plasma-assisted conversion of CO_2 in a dielectric barrier discharge reactor: understanding the effect of packing materials," *Plasma Sources Science and Technology*, vol. 24, no. 1, pp. 15011–15021, 2015.

[11] S. Paulussen, B. Verheyde, X. Tu, C. De Bie, T. Martens, D. Petrovic, A. Bogaerts, and B. Sels, "Conversion of carbon dioxide to value-added chemicals in atmospheric pressure dielectric barrier discharges," *Plasma Sources Science and Technology*, vol. 19, no. 3, pp. 034015 1–6, 2010.

[12] I. Belov, S. Paulussen, and A. Bogaerts, "Appearance of a conductive carbonaceous coating in a CO_2 dielectric barrier discharge and its influence on the electrical properties and the conversion efficiency," *Plasma Sources Science and Technology*, vol. 25, p. 015023, feb 2016.

[13] A. Berthelot and A. Bogaerts, "Modeling of CO_2 Splitting in a Microwave Plasma: How to Improve the Conversion and Energy Efficiency," *The Journal of Physical Chemistry C*, vol. 121, pp. 8236–8251, apr 2017.

[14] L. D. Pietanza, G. Colonna, G. D'Ammando, a. Laricchiuta, and M. Capitelli, "Vibrational excitation and dissociation mechanisms of CO_2 under non-equilibrium discharge and post-discharge conditions," *Plasma Sources Science and Technology*, vol. 24, no. 4, p. 042002, 2015.

[15] L. D. Pietanza, G. Colonna, G. D'Ammando, A. Laricchiuta, and M. Capitelli, "Electron energy distribution functions and fractional power transfer in "cold" and excited CO_2 discharge and post discharge conditions," *Physics of Plasmas*, vol. 23, no. 1, 2016.

[16] L. D. Pietanza, G. Colonna, G. D'Ammando, A. Laricchiuta, and M. Capitelli, "Non equilibrium vibrational assisted dissociation and ionization mechanisms in cold CO_2 plasmas," *Chemical Physics*, vol. 468, pp. 44–52, 2016.

[17] L. D. Pietanza, G. Colonna, V. Laporta, R. Celiberto, G. D'Ammando, A. Laricchiuta, and M. Capitelli, "Influence of Electron Molecule Resonant Vibrational Collisions over the Symmetric Mode and Direct Excitation-Dissociation Cross Sections of CO_2 on the Electron Energy Distribution Function and Dissociation Mechanisms in Cold Pure CO_2 Plasmas," *Journal of Physical Chemistry A*, vol. 120, no. 17, pp. 2614–2628, 2016.

[18] L. D. Pietanza, G. Colonna, G. D'Ammando, and M. Capitelli, "Time-dependent coupling of electron energy distribution function, vibrational kinetics of the asymmetric mode of CO_2 and dissociation, ionization and electronic excitation kinetics under discharge and post-discharge conditions," *Plasma Physics and Controlled Fusion*, vol. 59, no. 1, p. 014035, 2017.

[19] M. Capitelli, G. Colonna, G. D'Ammando, K. Hassouni, A. Laricchiuta, and L. D. Pietanza, "Coupling of Plasma Chemistry, Vibrational Kinetics, Collisional-Radiative Models and Electron Energy Distribution Function Under Non-Equilibrium Conditions," *Plasma Processes and Polymers*, pp. 1–11, 2016.

[20] R. Aerts, T. Martens, and A. Bogaerts, "Influence of Vibrational States on CO_2 Splitting by Dielectric Barrier Discharges," *The Journal of physical chemistry C*, vol. 116, pp. 23257–23273, 2012.

[21] T. Kozák and A. Bogaerts, "Splitting of CO_2 by vibrational excitation in non-equilibrium plasmas: a reaction kinetics model," *Plasma Sources Science and Technology*, vol. 23, p. 045004, aug 2014.

[22] T. Kozák and A. Bogaerts, "Evaluation of the energy efficiency of CO_2 conversion in microwave discharges using a reaction kinetics model," *Plasma Sources Science and Technology*, vol. 24, no. 1, p. 015024, 2015.

[23] R. Aerts, W. Somers, and A. Bogaerts, "Carbon Dioxide Splitting in a Dielectric Barrier Discharge Plasma: A Combined Experimental and Computational Study," *ChemSusChem*, vol. 8, no. 4, pp. 702–716, 2015.

[24] A. Bogaerts, C. De Bie, R. Snoeckx, and T. Kozák, "Plasma based CO_2 and CH_4 conversion: A modeling perspective," *Plasma Processes and Polymers*, vol. 14, p. e201600070, jun 2017.

[25] A. Bogaerts, W. Wang, A. Berthelot, and V. Guerra, "Modeling plasma-based CO_2 conversion : Crucial role of the dissociation cross section," *Plasma Sources Science and Technology*, vol. 25, pp. 1–23, 2016.

[26] S. Heijkers, R. Snoeckx, T. Kozák, T. Silva, T. Godfroid, N. Britun, R. Snyders, and A. Bogaerts, "CO_2 Conversion in a Microwave Plasma Reactor in the Presence of N_2: Elucidating the Role of Vibrational Levels," *The Journal of Physical Chemistry C*, vol. 119, no. 23, pp. 12815–12828, 2015.

[27] A. Berthelot and A. Bogaerts, "Modeling of plasma-based CO_2 conversion: lumping of the vibrational levels," *Plasma Sources Science and Technology*, vol. 25, no. 4, p. 045022, 2016.

[28] W. Wang, A. Berthelot, S. Kolev, X. Tu, and A. Bogaerts, "CO_2 conversion in a gliding arc plasma: 1D cylindrical discharge model," *Plasma Sources Science and Technology*, vol. 25, p. 065012, oct 2016.

[29] S. Ponduri, M. M. Becker, S. Welzel, M. C. M. Van De Sanden, D. Loffhagen, and R. Engeln, "Fluid

modelling of CO_2 dissociation in a dielectric barrier discharge," *Journal of Applied Physics*, vol. 119, no. 9, 2016.

[30] A. Janeco, N. R. Pinha, and V. Guerra, "Electron Kinetics in $He/CH_4/CO_2$ mixtures used for methane conversion," *Journal of Physical Chemistry C*, pp. 109–120.

[31] M. Grofulović, L. L. Alves, and V. Guerra, "Electron-neutral scattering cross sections for CO_2: a complete and consistent set and an assessment of dissociation," *J. Phys. D: Appl. Phys.*, vol. 49, p. 395207, 2016.

[32] A. V. Phelps, "Phelps Database retrieved from www.lxcat.net on September 4, 2014. http://jilawww.colorado.edu/~avp/."

[33] P. Koelman, S. Heijkers, S. Tadayon Mousavi, W. Graef, D. Mihailova, T. Kozák, A. Bogaerts, and J. van Dijk, "A Comprehensive Chemical Model for the Splitting of CO_2 in Non-Equilibrium Plasmas," *Plasma Processes and Polymers*, pp. 1–20, 2016.

[34] M. M. Turner, "Uncertainty and error in complex plasma chemistry models," *Plasma Sources Science and Technology*, vol. 24, p. 035027, jun 2015.

[35] M. M. Turner, "Uncertainty and sensitivity analysis in complex plasma chemistry models," *Plasma Sources Science and Technology*, vol. 25, p. 015003, feb 2016.

[36] M. M. Turner, "Computer Simulation in Low-Temperature Plasma Physics: Future Challenges," *Plasma Processes and Polymers*, p. 201600121, 2016.

[37] "S. Pancheshnyi, B. Eismann, G.J.M. Hagelaar, L.C. Pitchford, Computer code ZDPlasKin, http://www.zdplaskin.laplace.univ-tlse.fr (University of Toulouse, LAPLACE, CNRS-UPS-INP, Toulouse, France, 2008).."

[38] G. J. M. Hagelaar and L. C. Pitchford, "Solving the Boltzmann equation to obtain electron transport coefficients and rate coefficients for fluid models," *Plasma Sources Science and Technology*, vol. 14, pp. 722–733, nov 2005.

[39] I. Suzuki, "General anharmonic force constants of carbon dioxide," *Journal of Molecular Spectroscopy*, vol. 25, pp. 479–500, apr 1968.

[40] G. Herzberg, *Molecular Spectra and Molecular Structure: Spectra of Diatomic Molecules*. Princeton, NJ: Van Nostrand, 1950.

[41] H. G. Huber K, "NIST Chemistry WebBook, NIST Standard Reference Database Number 69 Constants of Diatomic Molecules," retrieved 4 December 2013.

[42] G. H. K. P. Huber, *Molecular Spectra and Molecular Structure IV. Constant of diatomic molecules*. Van Nostrand Rienhold Company, 1979.

[43] E. L. Crow and K. Shimizu, *Lognormal Distributions: Theory and Applications (Statistics: A Series of Textbooks and Monographs)*. CRC Press, 1987.

[44] M. Alvo and P. L. Yu, *Statistical Methods for Ranking Data*. No. 1976, New York, NY: Springer New York, 2014.

[45] I. V. Novobrantsev and A. N. Starostin, "Decay instability of vibrational relaxation in molecular gases," *Journal of Applied Mechanics and Technical Physics*, vol. 15, no. 2, pp. 283–285, 1974.

[46] D. Mcelroy, C. Walsh, A. J. Markwick, M. A. Cordiner, K. Smith, and T. J. Millar, "The UMIST database for astrochemistry 2012," *Astronomy & Astrophysics*, vol. 550, no. A36, 2013.

[47] "NIST Chemistry WebBook, NIST Standard Reference Database Number 69 Constants of Diatomic Molecules," retrieved 4 December 2013.

[48] L. C. Pitchford, L. L. Alves, K. Bartschat, S. F. Biagi, M.-c. Bordage, I. Bray, C. E. Brion, M. J. Brunger, L. Campbell, A. Chachereau, B. Chaudhury, L. G. Christophorou, E. Carbone, N. A. Dyatko, C. M. Franck, D. V. Fursa, R. K. Gangwar, V. Guerra, P. Haefliger, G. J. M. Hagelaar, A. Hoesl, Y. Itikawa, I. V. Kochetov, R. P. Mceachran, W. L. Morgan, A. P. Napartovich, V. Puech, M. Rabie, L. Sharma, R. Srivastava, A. D. Stauffer, J. Tennyson, J. D. Urquijo, J. V. Dijk, L. A. Viehland, M. C. Zammit, and O. Zatsarinny, "LXCat : an Open-Access , Web-Based Platform for Data Needed for Modeling Low Temperature Plasmas," *Plasma Processes and Polymers*, vol. 14, no. 1-2, 2017.

[49] M. Hayashi, *Swarm Studies and Inelastic Electron-Molecule Collisions*. New-York: Springer-

Verlag, 1987.

[50] C. Tian and C. R. Vidal, "Cross sections of the electron impact dissociative ionization of CO, CH_4 and C_2H_2," *Journal of Physics B: Atomic, Molecular and Optical Physics*, vol. 31, pp. 895–909, feb 1998.

[51] D. Rapp and D. D. Briglia, "Total Cross Sections for Ionization and Attachment in Gases by Electron Impact. II. Negative Ion Formation," *The Journal of Chemical Physics*, vol. 43, pp. 1480–1489, sep 1965.

[52] J. E. Land, "Electron scattering cross sections for momentum transfer and inelastic excitation in carbon monoxide," *Journal of Applied Physics*, vol. 49, pp. 5716–5721, dec 1978.

[53] S. A. Lawton and A. V. Phelps, "Excitation of the $b^1\Sigma_g^+$ state of O_2 by low energy electrons," *The Journal of Chemical Physics*, vol. 69, no. 3, p. 1055, 1978.

[54] C. S. Weller and M. A. Biondi, "Measurements of Dissociative Recombination of CO_2^+ Ions with Electrons," *Physical Review Letters*, vol. 19, pp. 59–61, jul 1967.

[55] J. Thoenes and S. C. Kurzius, "Plasma Chemistry Processes in the Closed Cycle EDL - Technical Report DRCPM-HEL-CR-79-11-VOL-1," tech. rep., Lockheed Missiles and Space Co Inc, Huntsville AL, 1979.

[56] T. G. Beuthe and J.-S. Chang, "Chemical Kinetic Modelling of Non-Equilibrium Ar-CO_2 Thermal Plasmas," *Japanese Journal of Applied Physics*, vol. 36, no. Part 1, No. 7B, pp. 4997–5002, 1997.

[57] J. B. A. Mitchell and H. Hus, "The dissociative recombination and excitation of CO^+," *Journal of Physics B: Atomic and Molecular Physics*, vol. 18, pp. 547–555, feb 1985.

[58] D. Albritton, "Ion-neutral reaction-rate constants measured in flow reactors through 1977," *Atomic Data and Nuclear Data Tables*, vol. 22, pp. 1–101, jul 1978.

[59] N. Adams, D. Smith, and D. Grief, "Reactions of H_nCO^+ ions with molecules at 300 K," *International Journal of Mass Spectrometry and Ion Physics*, vol. 26, pp. 405–415, apr 1978.

[60] F. C. Fehsenfeld and E. E. Ferguson, "Laboratory studies of negative ion reactions with atmospheric trace constituents," *The Journal of Chemical Physics*, vol. 61, no. 8, pp. 3181–3193, 1974.

[61] M. Mcfarland, D. L. Albritton, F. C. Fehsenfeld, E. E. Ferguson, and A. L. Schmeltekopf, "Flow-drift technique for ion mobility and ion-molecule reaction rate constant measurements. III. Negative ion reactions of O^- with CO, NO, H_2, and D_2," *Journal of Chemical Physics*, vol. 59, no. 12, pp. 6629–6635, 1973.

[62] D. Price and J. Moruzzi, "Negative ion molecule reactions in CO_2 at high pressures and temperatures," *Vacuum*, vol. 24, pp. 591–593, dec 1974.

[63] F. C. Fehsenfeld, A. L. Schmeltekopf, H. I. Schiff, and E. E. Ferguson, "Laboratory measurements of negative ion reactions of atmospheric interest," *Planetary and Space Science*, vol. 15, pp. 373–379, feb 1967.

[64] S. G. Belostotsky, D. J. Economou, D. V. Lopaev, and T. V. Rakhimova, "Negative ion destruction by $O(^3P)$ atoms and $O_2(a^1\Delta_g)$ molecules in an oxygen plasma," *Plasma Sources Science and Technology*, vol. 14, pp. 532–542, aug 2005.

[65] J. L. Pack and A. V. Phelps, "Electron Attachment and Detachment. II. Mixtures of O_2 and CO_2 and of O_2 and H_2O," *The Journal of Chemical Physics*, vol. 45, pp. 4316–4329, dec 1966.

[66] M. H. Bortner, T. Bourer, and C. A. Blank, "Defense Nuclear Agency Reaction Rate Handbook, Second Edition AD 763699," tech. rep., 1972.

[67] J. B. Hasted and R. A. Smith, "The Detachment of Electrons from Negative Ions," *Proceedings of the Royal Society A: Mathematical, Physical and Engineering Sciences*, vol. 235, pp. 349–353, may 1956.

[68] L. Frommhold, "Über verzögerte Elektronen in Elektronenlawinen, insbesondere in Sauerstoff und Luft, durch Bildung und Zerfall negativer Ionen (O^-)," *Fortschritte der Physik*, vol. 12, no. 11, pp. 597–642, 1964.

[69] J. T. Gudmundsson, "A critical review of the reaction set for a low pressure oxygen processing discharge RH-17-2004," tech. rep., University of Iceland, 2004.

[70] M. Burmeister and P. Roth, "ARAS measurements on the thermal decomposition of CO_2 behind

shock waves," *AIAA Journal*, vol. 28, pp. 402–405, mar 1990.

[71] D. L. Baulch, D. D. Drysdale, J. Duxbury, and S. Grant, *Evaluated Kinetic Data for High Temperature Reactions, Volume 3: Homogeneous Gas Phase Reactions of the O_2-O_3 System, the CO-O_2-H_2 System, and of the Sulphur-containing Species*. Butterworth, London, 1976.

[72] W. Tsang and R. F. Hampson, "Chemical Kinetic Data Base for Combustion Chemistry. Part I. Methane and Related Compounds," *Journal of Physical and Chemical Reference Data*, vol. 15, pp. 1087–1279, jul 1986.

[73] D. Husain and A. N. Young, "Kinetic investigation of ground state carbon atoms, $C(2^3P_J)$," *Journal of the Chemical Society, Faraday Transactions 2*, vol. 71, no. February, p. 525, 1975.

[74] R. R. Baldwin, D. Jackson, A. Melvin, and B. N. Rossiter, "The second limit of hydrogen + carbon monoxide + oxygen mixtures," *International Journal of Chemical Kinetics*, vol. 4, pp. 277–292, may 1972.

[75] A. J. Dean, D. F. Davidson, and R. K. Hanson, "A shock tube study of reactions of carbon atoms with hydrogen and oxygen using excimer photolysis of C_3O_2 and carbon atom atomic resonance absorption spectroscopy," *The Journal of Physical Chemistry*, vol. 95, pp. 183–191, jan 1991.

[76] C. J. S. M. Simpson, T. R. D. Chandler, and A. C. Strawson, "Vibrational Relaxation in CO_2 and CO_2–Ar Mixtures Studied Using a Shock Tube and a Laser–Schlieren Technique," *The Journal of Chemical Physics*, vol. 51, pp. 2214–2219, sep 1969.

[77] R. Taylor and S. Bitterman, "Survey of Vibrational Relaxation Data for Processes Important in the CO_2-N_2 Laser System," *Reviews of Modern Physics*, vol. 41, no. 1, pp. 26–47, 1969.

[78] J. A. Blauer and G. R. Gilmore, "A survey of vibrational relaxation rate data for processes important to CO_2-N_2-H_2O infrared plume radiation," *Ultrasystems, Inc. Technical Report*, pp. afrpl–tr–7, 1973.

[79] W. A. Rosser, A. D. Wood, and E. T. Gerry, "Deactivation of Vibrationally Excited Carbon Dioxide (ν_3) by Collisions with Carbon Dioxide or with Nitrogen," *The Journal of Chemical Physics*, vol. 50, pp. 4996–5008, jun 1969.

[80] K. F. Herzfeld, "Deactivation of Vibrations by Collision in the Presence of Fermi Resonance," *The Journal of Chemical Physics*, vol. 47, pp. 743–752, jul 1967.

[81] M. Capitelli, C. M. Ferreira, B. F. Gordiets, and A. I. Osipov, *Plasma kinetics in atmospheric gases*. Springer Berlin Heidelberg, springer s ed., 2000.

[82] R. D. Sharma, "Near Resonant Vibrational Energy Transfer among Isotopes of CO_2," *Physical Review*, vol. 177, no. 5, pp. 102–107, 1969.

[83] T. G. Kreutz, J. A. O'Neill, and G. W. Flynn, "Diode Laser Absorption Probe of Vibration-Vibration Energy Transfer in CO_2," *The Journal of Physical Chemistry*, vol. 91, no. 22, pp. 5540–5543, 1987.

[84] R. L. DeLeon and J. Rich, "Vibrational energy exchange rates in carbon monoxide," *Chemical Physics*, vol. 107, pp. 283–292, sep 1986.

[85] C. Flament, T. George, K. A. Meister, J. C. Tufts, J. W. Rich, V. V. Subramaniam, J. P. Martin, B. Piar, and M. Y. Perrin, "Nonequilibrium vibrational kinetics of carbon monoxide at high translational mode temperatures," *Chemical Physics*, vol. 163, no. 2, pp. 241–262, 1992.

Appendix A. List of chemical reactions included in the model

Table A1. Electron impact reactions calculated with cross sections data, using the calculated EEDF, as explained in part 2.2, as well as the references where the data are adopted from and the uncertainty of the data (expressed relative to the mean value). When not explicitly shown in the original source, the errors have been taken according to the values given by M. Hayashi [49].

No.	Reaction	Ref	$\frac{\Delta A}{A}$	Note
(X1)	$e + CO_2 \rightarrow 2e + CO_2^+$	[32]	0.1	
(X2)	$e + CO_2 \rightarrow 2e + O + CO^+$	[32]	0.3	
(X3)	$e + CO_2 \rightarrow O^- + CO$	[32]	0.3	
(X4)	$e + CO_2 \rightarrow e + O + CO$	[32]	0.3	
(X5)	$e + CO_2 \rightarrow e + CO_2^*$	[32]	0.3	
(X6)	$e + CO_2 \rightarrow e + CO_2 v_x$	[32]	0.3	x=a,b,c,d
(X7)	$e + CO_2 v \rightarrow e + CO_2 v_i$	[32]	0.3	
(X8)	$e + CO \rightarrow 2e + CO^+$	[50]	0.1	
(X9)	$e + CO \rightarrow C + O^-$	[51]	0.3	
(X9bis)	$e + CO \rightarrow e + C + O$	[52]	0.3	
(X10)	$e + CO \rightarrow e + CO(E_x)$	[52]	0.3	x=1,2,3,4
(X11)	$e + CO \rightarrow e + CO v_i$	[52]	0.3	i=1,2,3
(X12)	$e + O_2 \rightarrow e + O + O$	[53]	0.25	
(X12M)	$e + O_2 + M \rightarrow e + O_2^- + M$	[53]	0.25	
(X13)	$e + O_2 \rightarrow O + O^-$	[53]	0.25	
(X14)	$e + O_2 \leftrightarrow e + O_2 v_i$	[53]	0.25	i=1,2,3
(X17)	$e + O_2 \leftrightarrow e + O_2 E_i$	[53]	0.25	i=1,2

a) Same cross section also used for $CO_2 v_i$ (i = the various vibrationally excited levels)

b) Cross section also used for $CO_2 v_i$, modified by lowering the energy threshold by the energy of the excited state of $CO_2 v_i$

c) Cross section for the various levels (i,j) adopted from $e+CO_2 v_0 \rightarrow e+CO_2 v_1$, but scaled and shifted using Fridman's approximation

Table A2. Electron impact reactions using analytical expressions for the rate coefficients, given in m^3/s and m^6/s, for two-body and three-body reactions, respectively, as well as the references where the data are adopted from and the uncertainty of the data (expressed relative to the mean value). T_g and T_e are given in K and eV, respectively.

No.	Reaction	Rate coefficient	$\frac{\Delta A}{A}$	Reference
(E1a)	$e + CO_2^+ \rightarrow CO(v_1) + O$	$(1-\beta_{E1}) \times 2.0 \times 10^{-11} T_e^{-0.5} T_g^{-1}$	0.08	[54, 55]
(E1b)	$e + CO_2^+ \rightarrow C + O_2$	$\beta_{E1} \times k_{E1a} = \frac{k_{E1a}}{2}$		[56]
(E2)*	$e + CO_4^+ \rightarrow CO_2 + O_2$	$1.61 \times 10^{-13} T_e^{-0.5}$	0.3	[56]
(E3)	$e + CO^+ \rightarrow C + O$	$3.46 \times 10^{-14} T_e^{-0.48}$	0.25	[57, 46]
(E4)*	$e + O + M \rightarrow O^- + M$	1×10^{-43}	0.5	[55]

* The primary source was not accessible and/or the uncertainty was not given

Table A3. Ion-ion and ion-neutral reactions, as well as the references where the data are adopted from and the uncertainty of the data (expressed relative to the mean value). The rate coefficients are given in m^3/s and m^6/s, for two-body and three-body reactions, respectively. T_g is given in K.

No.	Reaction	Rate coefficient	$\frac{\Delta A}{A}$	Reference
(I1)	$CO_2 + CO^+ \rightarrow CO_2^+ + CO$	1.0×10^{-15}	0.2	[58, 59]
(I2a)[a]	$CO_2 + O^- + CO_2 \rightarrow CO_3^- + CO_2$	1.5×10^{-40}	0.3	[58, 60]
(I2b)[a]	$CO_2 + O^- + CO \rightarrow CO_3^- + CO$	1.5×10^{-40}	0.3	[58, 60]
(I2c)	$CO_2 + O^- + O_2 \rightarrow CO_3^- + O_2$	3.1×10^{-40}	0.3	[58, 60]
(I3)	$CO_2 + O_2^- + M \rightarrow CO_4^- + M$	4.7×10^{-41}	0.3	[58, 60]
(I4)	$CO + O^- \rightarrow CO_2 + e$	5.5×10^{-16}	0.3	[58, 61]
(I5)	$CO + CO_3^- \rightarrow 2CO_2 + e$	5×10^{-19}	0.2	[62]
(I6)*	$CO_3^- + CO_2^+ \rightarrow 2CO_2 v_b + O$	5×10^{-13}	0.5	[55]
(I7)*	$CO_4^- + CO_2^+ \rightarrow 2CO_2 v_b + O_2$	5×10^{-13}	0.5	[55]
(I8)*	$O_2^- + CO_2^+ \rightarrow CO_2 v_1 + O_2 + O$	6×10^{-13}	0.5	[55]
(I9)	$CO_3^- + O \rightarrow CO_2 + O_2^-$	8×10^{-17}	1	[63]
(I10a)*	$CO_4^- + O \rightarrow CO_3^- + O_2 + O$	1.12×10^{-16}	1	[58]
(I10b)*	$CO_4^- + O \rightarrow CO_2 + O_2 + O^-$	1.4×10^{-17}	1	[58]
(I11)	$O + O^- \rightarrow O_2 + e$	2.3×10^{-16}	0.2	[64]
(I12)*	$O + O_2^- \rightarrow O_2 + O^-$	1.5×10^{-16}	1	[58]
(I13)	$O_2^- + M \rightarrow O_2 + M + e$	$2.7 \times 10^{-16} (\frac{T_g}{300})^{0.5} exp(-5590/T_g)$	0.11	[65, 66]
(I14)[b]	$O^- + M \rightarrow O + M + e$	$2.3 \times 10^{-15} exp(-26000/T_g)$	0.5	[67, 68, 66]

* The primary source was not accessible and/or the uncertainty was not given

[a] The rate coefficient of $CO_2 + O^- + He \rightarrow CO_3^- + He$ was used, due to the lack of further information.

[b] For usual values of gas temperature, i.e. $T_g \ll 26000$ K, the rate coefficient is very low, as pointed out by Gudmundsson [69].

Table A4. Neutral-neutral reactions, as well as the references where the data are adopted from and the uncertainty of the data (expressed relative to the mean value). The rate coefficients are given in m^3/s and m^6/s, for two-body and three-body reactions, respectively. T_g is given in K. The α parameter determines the effectiveness of lowering the activation energy for reaction involving vibrationally excited levels of the molecules (see details in [2, 21]).

No.	Reaction	Rate coefficient	$\frac{\Delta A}{A}$	α	References*
(N1)	$CO_2 + M \rightarrow CO + O + M$	$6.06 \times 10^{-16} exp(-52525/T_g)$	0.15	0.8	[70]
(N2)[a]	$CO_2 + O \rightarrow CO + O_2$	$2.8 \times 10^{-17} exp(-26500/T_g)$	2	0.5	[71, 72]
(N3)[b]	$CO_2 + C \rightarrow 2CO$	$< 10^{-21}$	-	n.a.	[73]
(N4)[c]	$CO + O + M \rightarrow CO_2 + M$	$8.3 \times 10^{-46} exp(-1510/T_g)$	1	0.0	[74, 72]
(N5)[a]	$O_2 + CO \rightarrow CO_2 + O$	$4.2 \times 10^{-18} exp(-24000/T_g)$	1	0.5	[72]
(N6)	$O_2 + C \rightarrow CO + O$	$1.99 \times 10^{-16} exp(-2010/T_g)$	0.5	0.0	[75]
(N7)[d]	$O + C + M \rightarrow CO + M$	$2.14 \times 10^{-41} (\frac{T_g}{300})^{-3.08} exp(-2144/T_g)$	2	n.a.	[71, 72]
(N8)[e]	$O + O + M \rightarrow O_2 + M$	$5.2 \times 10^{-47} exp(900/T_g)$	0.3	n.a.	[71, 72]
(N9)[e]	$O_2 + M \rightarrow O + O + M$	$3.0 \times 10^{-12} \frac{1}{T_g} exp(-59380/T_g)$	0.3	0.0	[71, 72]

* Baulch et al.[71] and Tsang et al.[72] are reviews assessing the reliability of different sources. Baulch et al.[71] derived rate coefficient expressions based on different sources and gave a value for the error. We consider it to be the primary source.

[a] Baulch et al.[71] suggests that $\frac{\Delta A}{A}$ is 1 at 1500 K and 0.5 at 3000 K. Tsang et al.[72] suggests $\frac{\Delta A}{A} = 2$.

[b] A rate coefficient is randomly chosen between 0 and 10^{-21} m^3/s, the maximum value.

[c] Multiply by 7, 3 or 12 for M= CO_2, CO or O_2 respectively; Baldwin et al.[74] suggests that $\frac{\Delta A}{A}$ is 0.2 at $T_g = 300$ K and 1 at $T_g = 800$ K.

[d] Baulch et al.[71] gives an uncertainty $\frac{\Delta A}{A} = 0.75$ at 7000 K. We have thus chosen a larger uncertainty, since the temperatures in this work are much lower.

[e] Baulch et al.[71] gives $\frac{\Delta A}{A} = 0.2$ at 190 K and 0.6 at 4000 K. Given the typical temperature values used, we chose a value of 0.3.

Table A5. Neutral reactions between vibrationally excited molecules, as well as the references where the data are adopted from and the uncertainty of the data (expressed relative to the mean value). The rate coefficients are given in m^3/s and m^6/s, for two-body and three-body reactions, respectively. T_g is given in K.

No.	Reaction	Rate coefficient	$\frac{\Delta A}{A}$	References*
(V1)	$CO_2v_a + M \rightarrow CO_2 + M$	$7.14 \times 10^{-15}\, exp(-177\, T_g^{-1/3} + 451\, T_g^{-2/3})$	0.3	[76, 77, 78]
(V2a)	$CO_2v_1 + M \rightarrow CO_2v_a + M$	$4.25 \times 10^{-7}\, exp(-407\, T_g^{-1/3} + 824\, T_g^{-2/3})$	0.1	[79, 80, 78]
(V2b)	$CO_2v_1 + M \rightarrow CO_2v_b + M$	$8.57 \times 10^{-7}\, exp(-404\, T_g^{-1/3} + 1096\, T_g^{-2/3})$	0.1	[79, 80, 78]
(V2c)	$CO_2v_1 + M \rightarrow CO_2v_c + M$	$1.43 \times 10^{-7}\, exp(-252\, T_g^{-1/3} + 685\, T_g^{-2/3})$	0.1	[79, 80, 78]
(V3)	$COv_1 + M \rightarrow CO + M$	$1.0 \times 10^{-18}\, T_g\, exp(-150.7\, T_g^{-1/3})$	0.15	[81]
(V4)	$O_2v_1 + M \rightarrow O_2 + M$	$1.3 \times 10^{-14}\, exp(-158.7\, T_g^{-1/3})$	0.1	[77, 78]
(V5)	$CO_2v_1 + CO_2 \rightarrow CO_2v_a + CO_2v_b$	$1.06 \times 10^{-11}\, exp(-242\, T_g^{-1/3} + 633\, T_g^{-2/3})$	0.1	[79, 80, 78]
(V6)	$CO_2v_1 + CO_2 \rightarrow CO_2 + CO_2v_1$	$1.32 \times 10^{-18}\, (\frac{T_g}{300})^{0.5} \frac{250}{T_g}$	0.1	[82, 83]
(V7)	$COv_1 + CO \rightarrow CO + COv_1$	$3.4 \times 10^{-16} (\frac{T_g}{300})^{0.5} (1.64 \times 10^{-6}\, T_g + \frac{1.61}{T_g})$	0.1	[84, 85]
(V8)	$CO_2v_1 + CO \rightarrow CO_2 + COv_1$	$4.8 \times 10^{-12}\, exp(-153\, T_g^{-1/3})$	0.1	[79, 78]

* Blauer and Gilmore [78] collected data from different sources and derived analytical expressions for the rate coefficients, without assessing the uncertainty. We estimated the value of $\frac{\Delta A}{A}$ based on the primary source of the data.